ARTICLES
https://doi.org/10.1038/s41567-022-01508-z

nature physics

Microscopic origin of excess wings in relaxation spectra of supercooled liquids

Benjamin Guiselin[1,4], Camille Scalliet[2,4] and Ludovic Berthier[1,3] ✉

Glass formation is encountered in diverse materials. Experiments have revealed that the dynamic relaxation spectra of supercooled liquids generically become asymmetric near the glass transition temperature T_g, where an extended power law emerges at high frequencies. The microscopic origin of this 'wing' remains unknown, and has so far been inaccessible to simulations. Here we develop a novel computational approach and study the equilibrium dynamics of model supercooled liquids near T_g. We demonstrate the emergence of a power-law wing in the numerical spectra, which originates from relaxation at rare, localized regions over broadly distributed timescales. We rationalize the asymmetric shape of the relaxation spectra by constructing an empirical model associating heterogeneous activated dynamics with dynamic facilitation, which are the two minimal physical ingredients revealed by our simulations. Our work offers a glimpse into the molecular motion responsible for glass formation at relevant experimental conditions.

The formation of amorphous solids results from the rapid growth of structural relaxation time τ_α of a supercooled liquid[1]. Molecular motion occurs on a timescale of about 10^{-10} s at the onset temperature of glassy behaviour, but it takes about 100 s at the experimental glass transition temperature T_g (ref. [2]). Over the last decades, dielectric, mechanical and light-scattering experiments kept developing to probe molecular motion over a broader frequency range with increased accuracy[3–8]. This progress reveals that the temperature evolution of τ_α is just the tip of the iceberg, as relaxation spectra $\chi''(\omega)$ measured near T_g exhibit relaxation processes taking place over an extremely large frequency window[9–12]. The overall shift in the relaxation spectra is accompanied by an equivalent broadening of about 12 decades, which is the other side of the same coin. A microscopic explanation of these slow dynamics is at the heart of glass transition research[1].

High-temperature spectra reflect near-exponential relaxation in the picosecond range, but low-temperature spectra broaden into a two-step process with a stretched exponential relaxation at low frequency $\omega \approx 1/\tau_\alpha$ and a microscopic peak remaining at the picosecond timescale. In 1990, more precise experiments[11–14] showed that for a number of molecular liquids, the structural relaxation peak extends much further at higher frequencies $\omega\tau_\alpha \gg 1$ and transforms into a power law, namely, $\chi''(\omega) \approx \omega^{-\sigma}$, with a small exponent $\sigma(T) \in [0.2, 0.4]$ decreasing with temperature[14]. Using logarithmic scales, this resembles a 'wing' in 'excess' of the α peak. At T_g, the wing extends over the millihertz–megahertz range with an amplitude about 100 times smaller than the α peak. A universal scaling comprising the excess wing was proposed[14], which can be altered by further microscopic processes[15,16]. Although this universality is debated[9,10], the presence of an excess contribution often taking the form of a wing is not[6,17].

Elucidating the nature of molecular motion responsible for the small signal in these excess wings appears daunting. Yet, experiments managed to characterize its heterogeneous nature[18,19] and aging properties[20]. So far, computer simulations were unable to access the required range of equilibration temperatures and timescales to even address the question. Physical interpretations and empirical models have been proposed to explain the shape of the relaxation spectra. Some of them couple slow translational motion with an 'additional' degree of freedom (for example, rotational)[21,22]. Others invoke spatially heterogeneous dynamics to construct a broad distribution of timescales of static[23–27] or kinetic[28] origin. The winged asymmetric shape then requires specific physics, such as geometric frustration[25], length-scale-dependent dynamics[26] or dynamic facilitation[28]. With specific choices, these approaches yield relaxation spectra comprising excess wings, but direct microscopic investigations testing the underlying hypotheses are still lacking.

Here we show that computer simulations can now directly observe excess wings and assess their microscopic origin. We take advantage of the recent swap Monte Carlo algorithm[29] to efficiently produce equilibrated configurations of a supercooled liquid with $\tau_\alpha \approx 100$ s. We observe their physical relaxation dynamics over 10 decades in time, up to 20 ms. We are, thus, able to probe the temperature and time regimes where excess wings are observed in experiments. We report the emergence of a power law (a wing) in the numerical spectra with the same characteristics as in experiments. We demonstrate that it is caused by a sparse population of localized regions, whose relaxation times follow a power-law distribution. These relaxed regions then coarsen by dynamic facilitation. We construct an empirical model to illustrate how heterogeneous dynamics and dynamic facilitation generically lead to asymmetric, winged relaxation spectra.

We study size-polydisperse mixtures of N soft repulsive spheres in two and three dimensions (Methods). These models are representative computational glass formers[30,31]. We use the swap Monte Carlo algorithm (designed in ref. [32]) to generate $n_s \in [200, 450]$ independent equilibrium configurations at temperature T down to the extrapolated experimental glass transition temperature T_g. Each equilibrium configuration is then taken as the initial condition of a multiple central processing unit (CPU) molecular dynamics (MD) simulation (without swap). The n_s independent simulations run for up to a simulation time t_{max} of 1.5×10^7 in

[1]Laboratoire Charles Coulomb (L2C), Université de Montpellier, CNRS, Montpellier, France. [2]Department of Applied Mathematics and Theoretical Physics, University of Cambridge, Cambridge, UK. [3]Yusuf Hamied Department of Chemistry, University of Cambridge, Cambridge, UK. [4]These authors contributed equally: Benjamin Guiselin, Camille Scalliet. ✉e-mail: ludovic.berthier@umontpellier.fr

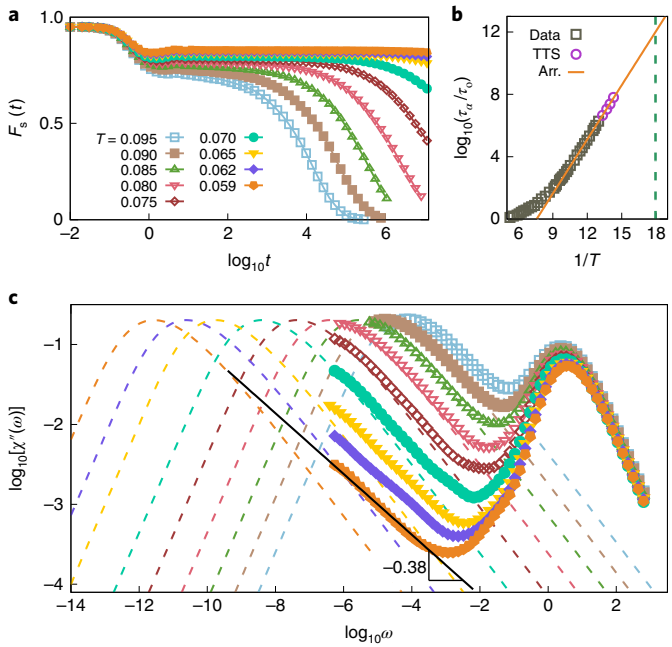

Fig. 1 | Emergence of excess wings in a 3D glass former near the glass transition temperature. a, Self-intermediate scattering function $F_s(t)$ at various temperatures. **b**, Relaxation time τ_α rescaled by its value τ_o at the onset temperature. The symbols are directly measured data (squares) or obtained using TTS (circles). A conservative Arrhenius extrapolation (Arr.) locates $T_g = 0.056$, where $\tau_\alpha(T_g)/\tau_o = 10^{12}$ (dashed line). **c**, Relaxation spectra for the same temperatures as in **a**. The dashed lines represent the estimated α peaks. Close to T_g, the spectra lie above the α peak and display a power-law signal with an exponent $\sigma \approx 0.38$ (full line), in quantitative agreement with the experimentally observed excess wings.

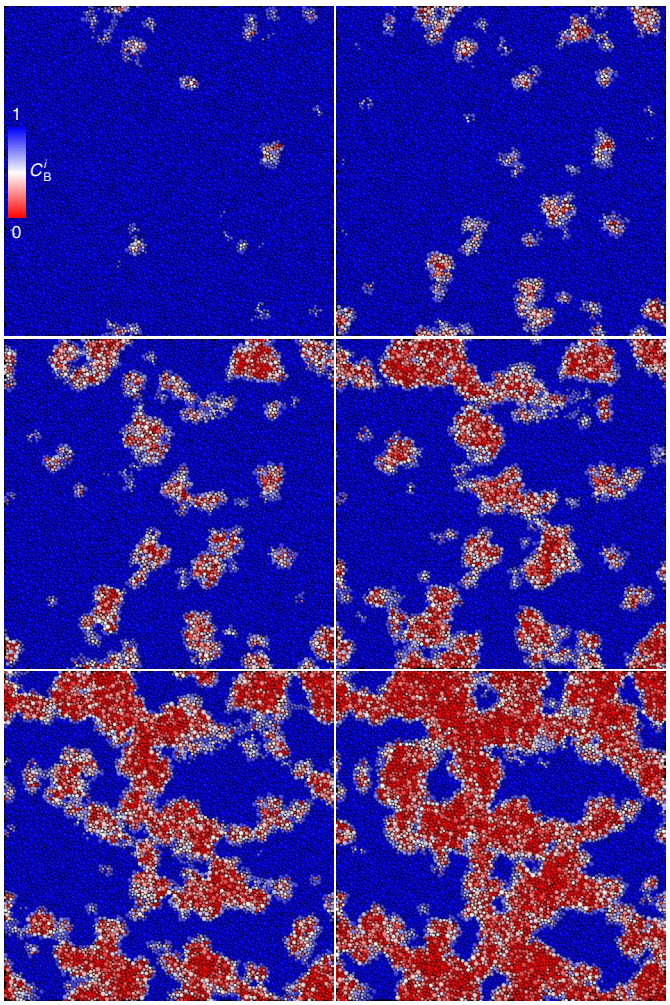

Fig. 2 | Visualization of spatially heterogeneous and facilitated dynamics. Relaxation in the 2D system at $T_{2D} = 0.09$ with $\tau_\alpha/\tau_o = 10^8$. Frames are logarithmically spaced between $t = 2\times10^{-3}\tau_\alpha$ (top left) and $t = 0.6\tau_\alpha$ (bottom right) from left to right and top to bottom. The particles are coloured according to $C_B^i(t)$ from blue (immobile; $C_B^i(t) = 1$) to red (relaxed; $C_B^i(t) = 0$). The linear size of the simulation box is 100.

three dimensions (one week on two CPUs for $N = 1{,}200$). We push a few two-dimensional (2D) simulations to unprecedentedly long times, up to $t_{max,2D} = 6\times10^8$, representing a computational time of several months. By using the relaxation time at the onset of glassy dynamics to relate the numerical and experimental timescales, our longest simulations translate into a physical time of about 20 ms for systems having an equilibrium relaxation time $\tau_\alpha \approx 10^2$ s. This strategy is the key to observe excess wings, which would otherwise be buried underneath structural relaxation in conventional approaches[33]. The 2D and three-dimensional (3D) models behave similarly; therefore, we present quantitative results for the 3D model ($N = 1{,}200$) in Figs. 1 and 3 and illustrate the relaxation process in Fig. 2 with 2D snapshots ($N = 10{,}000$), which are easier to visualize. Quantitative results for the 2D model are provided in the Supplementary Information.

We investigate the spatiotemporal evolution of the relaxation dynamics using averaged and particle-resolved dynamic observables. In three dimensions, we measure the self-intermediate scattering function $F_s(t)$, averaged over the n_s independent runs. We define the relaxation time τ_α by $F_s(\tau_\alpha) = e^{-1}$. In two dimensions, collective long-ranged fluctuations affect the measurement of $F_s(t)$. We instead focus on observables that are independent of these fluctuations[34] and define τ_α via the bond-orientational correlation function[35]. In both two and three dimensions, we investigate the relaxation process at the particle scale via the bond-breaking correlation $C_B^i(t)$ that quantifies the fraction of nearest neighbours lost by particle i after time t. Starting from $C_B^i(t = 0) = 1$, it decreases as rearrangements take place close to particle i, and reaches zero when its local environment is completely renewed. Precise definitions of the correlation functions are provided in Methods.

To connect with experimental results obtained in the frequency domain, we compute the dynamic susceptibility $\chi''(\omega)$ from a distribution of relaxation times $G(\log\tau)$ (refs.[17,28]):

$$\chi''(\omega) = \int_{-\infty}^{\infty} G(\log\tau)\frac{\omega\tau}{1+(\omega\tau)^2}\mathrm{d}\log\tau\ , \qquad (1)$$

where distribution G is related to the derivative of a time correlation function, $G(\log t) \approx -\mathrm{d}F_s(t)/\mathrm{d}\log t$ in three dimensions. We use the bond-breaking correlation function instead of F_s in two dimensions. We discuss the numerical evaluation of χ'' in Methods, and discussion on the statistical noise and comparison with direct Fourier transforms are provided in Supplementary Section I and Supplementary Figs. 1 and 2.

We start by presenting the equilibrium measurements of $F_s(t)$ in three dimensions (Fig. 1a), concentrating on the unexplored low-T regime below the mode-coupling crossover $T_{mct} \approx 0.095$. The latter is determined by a power-law fit of $\tau_\alpha(T)$ in the range $\tau_\alpha/\tau_o < 10^3$, where $\tau_o \approx 3$ is the value of τ_α at the onset temperature $T_o \approx 0.20$ (ref. [29]). At all the temperatures, the correlations display a fast initial decay near $t \approx \tau_o$, due to fast dynamical processes. At larger times, we observe

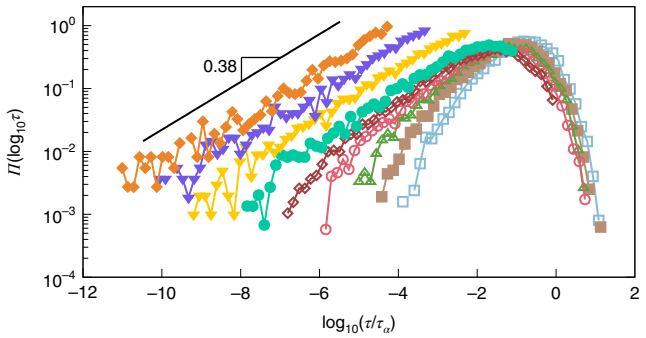

Fig. 3 | Microscopic origin of excess wings. Waiting-time distribution of newly relaxing clusters in three dimensions from T_{mct} (right) to T_g (left), with the same colour code as Fig. 1a. Approaching T_g, the distributions develop a power-law tail at $\tau \ll \tau_\alpha$, with an exponent of 0.38 that directly accounts for the excess wings in the spectra of Fig. 1c.

a much slower decay to zero. As T decreases, the relaxation time grows and eventually exits the numerically accessible time window. At the lowest investigated temperatures near T_g, correlations appear almost constant over more than seven decades in time, suggesting a near-complete dynamic arrest. We recall that owing to the swap algorithm, all the measurements reflect genuine equilibrium dynamics, even when τ_α is larger than the simulated time by many orders of magnitude.

Our strategy allows us to directly observe the α relaxation when $\tau_\alpha < t_{max}$; equivalently, $\tau_\alpha/\tau_o \lesssim 5\times10^6$ down to $T=0.0755$ (Figs. 1a,b). In this regime, the relaxation is well described by a stretched exponential $F_0 e^{-(t/\tau_\alpha)^\beta}$ with an almost constant stretching exponent $\beta \approx 0.56$, and amplitude F_0 that changes modestly with temperature. We use this time–temperature superposition (TTS) property to estimate τ_α for $0.0700 \le T \le 0.0755$, where the decorrelation of $F_s(t)$ is sufficient[36], and obtain τ_α over roughly two more decades (Fig. 1b). We finally use an Arrhenius law to extrapolate τ_α over four more decades to get a safe lower bound for the experimental glass transition temperature $T_g \approx 0.056$, defined by $\tau_\alpha(T_g)/\tau_o = 10^{12}$ (ref. [29]; Methods).

The corresponding relaxation spectra are shown in Fig. 1c for the 3D model. All of them display a peak at high frequency $\omega \approx 1/\tau_o$, corresponding to the short-time decay of $F_s(t)$. A low-frequency peak near $\omega \approx 1/\tau_\alpha$ is also visible. As T decreases, this α peak shifts to lower frequencies and eventually exits the accessible frequency window. When the α peak is not directly measured, we extrapolate its shape by inserting the above stretched exponential form for $F_s(t)$ into equation (1). We use $\beta=0.56$; τ_α is given by the Arrhenius extrapolation and constant F_0. The tiny temperature dependence of F_0 is immaterial on a logarithmic scale (Fig. 1c). The resulting α peaks are shown in Fig. 1c with dashed lines that smoothly merge into the measured data at the highest temperatures, validating our procedure.

As T decreases, the measured susceptibility and α peak deviate increasingly from one another, the data being systematically in excess of the α peak. Since the Arrhenius extrapolation underestimates τ_α, this excess is (at worst) slightly underestimated and cannot be accounted for by a vertical shift that would require unphysical values of F_0 and β. At the lowest T, where the α peak no longer interferes with the measurements, the spectra are well described by a power law $\chi''(\omega) \approx \omega^{-\sigma}$ at low frequencies, with exponent $\sigma \approx 0.38$ slightly decreasing with T, and an amplitude about 100 times smaller than the α peak. The relaxation spectra of the 2D model (Supplementary Fig. 3) exhibit similar features with exponent $\sigma_{2D} \approx 0.45$, which is fairly close to the one found in three dimensions. In our simulations, the measured spectra do not exhibit a secondary peak separated from the α relaxation, and cannot be interpreted using an additive β process[33]. Therefore, close to T_g, the numerical spectra follow a power law over a similar frequency range, with a similar exponent and similar amplitude as the excess wings obtained experimentally, suggesting that simulated glass formers display excess wings resembling observations in molecular liquids.

We take advantage of the atomistic resolution offered by simulations to explore the microscopic origin of excess wings and provide a physical interpretation of the spectral shapes. We illustrate the relaxation dynamics with 2D snapshots, which are easier to render and interpret. We confirm that the same mechanisms are observed in three dimensions. In Fig. 2, we show the 2D snapshots illustrating how structural relaxation proceeds at temperature $T_{2D}=0.09$ (we estimate $T_{g,2D} \approx 0.07$) for which $\tau_\alpha/\tau_o \approx 10^8$, which corresponds to around 10 ms in physical time. This temperature is the lowest for which the α relaxation can be observed in the numerical window, and is considerably lower than the mode-coupling crossover near $T_{mct,2D} \approx 0.12$. The images are shown at logarithmically spaced times t in the range $t/\tau_\alpha \in [10^{-3}, 1]$. The particles are coloured according to $C_B^i(t)$: red particles have relaxed and blue ones have not. Supplementary Fig. 3 shows the relaxation spectrum measured at this temperature.

For $t \ll \tau_\alpha$, relaxation starts at a sparse population of localized regions that independently emerge throughout the sample over broadly distributed times. This conclusion holds over a large range of temperatures down to T_g for both $d=2$ and $d=3$. As time increases, newly relaxed regions continue to appear, but a second mechanism becomes apparent (Fig. 2) as regions that have relaxed in one frame typically appear larger in the next. This growth of relaxed regions (Fig. 2) is the signature of dynamic facilitation[37]. More precisely, we observe that from one frame to the next, relaxation events keep accumulating at similar locations, which results in mobile particles undergoing multiple relaxations and mobility propagating to nearby particles. Also, the slowest regions are typically 'invaded' at $t \gg \tau_\alpha$ from their faster boundaries. Dynamic facilitation has been identified before at high temperatures above the mode-coupling crossover[37–39]. Our investigations show that it becomes a central physical mechanism for structural relaxation near T_g.

We concentrate on the early times where the power-law spectra are observed. The visualization suggests that clusters of relaxed particles appear at sparse locations. We now establish that these early relaxation events are responsible for the excess wing. To this end, we define mobile ($C_B^i(t) < 0.55$) and immobile ($C_B^i(t) \ge 0.55$) particles; the threshold value near 0.50 is determined requiring self-consistency with alternative mobility definitions based on displacements. We identify connected clusters of mobile particles by performing a nearest-neighbour analysis (Methods), and investigate the statistical properties of relaxed clusters. In particular, we find that the excess wing regime at $t/\tau_\alpha \ll 1$ is dominated by the appearance of new clusters, whereas the growth of existing clusters dominates at later times. Figure 3 shows the distribution $\Pi(\tau)$ of waiting times τ for the appearance of new clusters in three dimensions. For $T \le 0.07$, we cannot measure the entire distribution, which is, thus, determined up to an uninteresting prefactor. The corresponding 2D results are shown in Supplementary Fig. 4.

At the highest investigated temperature, near T_{mct}, the distribution $\Pi(\log_{10}\tau)$ in Fig. 3 is already very broad, with clusters appearing as early as $10^{-4}\tau_\alpha$. The distribution peaks near $0.1\tau_\alpha$, when dynamic facilitation starts to dominate, and has a cutoff at around $10\tau_\alpha$. As T decreases below the mode-coupling crossover, a power-law tail emerges at $\tau \ll \tau_\alpha$. For $T \le 0.07$, the power law extends over at least six decades, with a nearly constant exponent $\Pi(\log_{10}\tau) \approx \tau^{0.38}$ for the 3D model. The relaxation of localized clusters at early times is extremely broadly distributed, presumably stemming from an equally broad distribution of activation energies.

Remarkably, if we plug the measured distribution of waiting times in equation (1), the power law $\Pi(\log_{10}\tau) \approx \tau^{0.38}$ directly

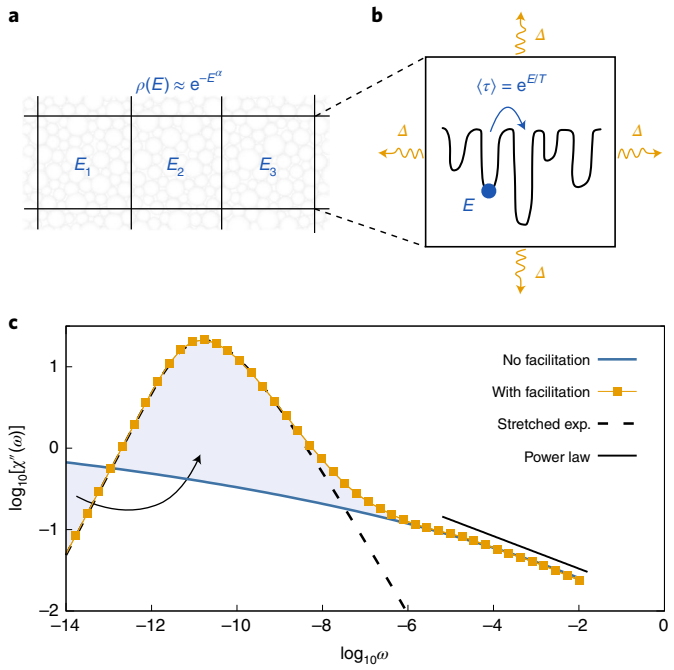

Fig. 4 | Facilitated trap model generically predicts asymmetric winged relaxation spectra. a, The liquid is modelled as a collection of traps with energies E, distributed according to $\rho(E)$. **b**, Relaxation is thermally activated and affects the energy of the other traps by a random amount, proportional to Δ. **c**, Relaxation spectra $\chi''(\omega)$ in the absence ($\Delta = 0$) and presence ($\Delta = 0.05$) of dynamic facilitation at $\alpha = 1.1$ and $T = 0.629$. Dynamic facilitation compresses (arrow) the low-frequency part of the underlying spectrum, giving rise to a sharper α peak well fitted by the spectrum of a stretched exponential (dashed). The high-frequency part of the underlying spectrum, unaffected by facilitation, is well described by a power law, namely, $\omega^{-0.2}$ (line). The excess wing, thus, corresponds to the beginning of the relaxation process.

translates into a power law $\chi''(\omega) \approx \omega^{-0.38}$ in the spectra, which is, thus, valid for $\omega\tau_\alpha \gg 1$. The agreement with the data in Fig. 1c is, therefore, quantitative. A similar agreement is found in two dimensions with the exponent $\sigma_{2D} = 0.45$ (Supplementary Fig. 4). This analysis demonstrates that the high-frequency power law in $\chi''(\omega)$ stems from the relaxation of a sparse population of clusters characterized by a broad distribution of relaxation times.

This microscopic view of the power-law wing alone does not explain why it appears in excess of the α peak observed at larger times where dynamic facilitation is observed. To explain this point, we construct an empirical model based on our numerical observations. We first imagine that the liquid can be decomposed into independent domains characterized by a local relaxation time (Fig. 4a). This heterogeneous viewpoint is mathematically captured by trap models[40,41]. To introduce dynamic facilitation as the second key ingredient, we construct a facilitated trap model, assuming that a given local relaxation event may now affect the state of the other traps (Fig. 4b). To provide a qualitative, generic description of the relaxation spectra, we analyse the simplest version of such a model and assume, in a mean-field spirit, that dynamic facilitation equally affects all the traps. A more local version was designed elsewhere[42,43] for different purposes.

We consider N traps with energy levels $E > 0$ drawn from distribution $\rho(E)$, and assume an activated dynamics. The energy E of a trap is renewed after a Poisson-distributed timescale of mean $\langle\tau(E)\rangle = e^{E/T}$. Since deep traps take much longer to relax than shallow ones, the system is dynamically heterogeneous. Following ref. [44], we use $\rho(E) \propto e^{-E^\alpha}$, where $\alpha \in [1, 2]$, to smoothly interpolate between the much-studied Gaussian[40,42] and exponential[41] distributions. The dynamics at temperature T leads to the equilibrium energy distribution $P_{eq}(T, E) \propto \rho(E)e^{E/T}$. Whenever a trap relaxes, the energy of all the other traps is shifted by a random amount uniformly distributed in the interval $\left[-\frac{\Delta}{\sqrt{N}}, \frac{\Delta}{\sqrt{N}}\right]$, using a Metropolis filter to leave the equilibrium distribution P_{eq} unchanged. This coupling between traps mimics dynamic facilitation[42]. The relaxation spectra $\chi''(\omega)$ is computed either analytically ($\Delta = 0$) or by simulating the facilitated model ($\Delta > 0$).

The model is specified by two parameters, namely, α and Δ, for which equilibrium dynamics can be studied at any temperature T. We have systematically investigated this parameter space, and find spectra with quantitative differences but generic features[45]. In Fig. 4c, we select $\alpha = 1.1$ and $\Delta = 0.05$ at $T = 0.629$ for aesthetic reasons, as this produces a spectrum qualitatively resembling the experimental and numerical ones close to T_g. Fitting the α peak to the frequency representation of a stretched exponential reveals an excess wing at high frequencies. However, in the absence of dynamic facilitation ($\Delta = 0$), one obtains the blue spectrum (Fig. 4c), with the same high-frequency behaviour, but which extends much further at low frequencies. Indeed, without facilitation, each trap relaxes independently, and the equilibrium distribution P_{eq} determines the dynamic spectrum, which is broad and relatively symmetric. In the presence of facilitation ($\Delta > 0$), shallow traps still relax independently and are essentially unaffected. Crucially, deep traps now receive small kicks whenever a shallow trap relaxes, and their energies slowly diffuse towards the most probable value. This accelerates their relaxation, which eventually affects the tail of the relaxation time distribution. As a result, dynamic facilitation 'compresses' the low-frequency part of the underlying spectrum (blue), as hinted in ref. [46], and highlighted by the arrow in Fig. 4c. We, thus, interpret the winged, asymmetric spectrum as a broad underlying distribution of relaxation timescales (well described by a power law at early times) compressed by dynamic facilitation at long times. Ironically, in our picture, the α peak itself is in 'excess' of a much broader underlying time distribution with a high-frequency power-law shape. In this view, the excess wing forms an integral part of the structural relaxation.

Our study frontally attacks a central question regarding the relaxation dynamics of supercooled liquids near the experimental glass transition and paves the way for many more studies of a totally unexplored territory now made accessible to modern computer studies. Further enlarging the family of available computer glass formers would also help filling the gap with more complex molecular systems studied experimentally.

Online content

Any methods, additional references, Nature Research reporting summaries, source data, extended data, supplementary information, acknowledgements, peer review information; details of author contributions and competing interests; and statements of data and code availability are available at https://doi.org/10.1038/s41567-022-01508-z.

Received: 23 March 2021; Accepted: 7 January 2022;
Published online: 17 March 2022

References

1. Berthier, L. & Biroli, G. Theoretical perspective on the glass transition and amorphous materials. *Rev. Mod. Phys.* **83**, 587 (2011).
2. Schmidtke, B., Petzold, N., Kahlau, R., Hofmann, M. & Rössler, E. A. From boiling point to glass transition temperature: transport coefficients in molecular liquids follow three-parameter scaling. *Phys. Rev. E* **86**, 041507 (2012).

3. Lunkenheimer, P., Schneider, U., Brand, R. & Loid, A. Glassy dynamics. *Contemp. Phys.* **41**, 15–36 (2000).
4. Körber, T., Stäglich, R., Gainaru, C., Böhmer, R. & Rössler, E. A. Systematic differences in the relaxation stretching of polar molecular liquids probed by dielectric vs magnetic resonance and photon correlation spectroscopy. *J. Chem. Phys.* **153**, 124510 (2020).
5. Schmidtke, B., Petzold, N., Kahlau, R. & Rössler, E. A. Reorientational dynamics in molecular liquids as revealed by dynamic light scattering: from boiling point to glass transition temperature. *J. Chem. Phys.* **139**, 084504 (2013).
6. Gainaru, C., Kahlau, R., Rössler, E. A. & Böhmer, R. Evolution of excess wing and β-process in simple glass formers. *J. Chem. Phys.* **131**, 184510 (2009).
7. Flämig, M., Hofmann, M., Fatkullin, N. & Rössler, E. A. NMR relaxometry: the canonical case glycerol. *J. Phys. Chem. B* **124**, 1557–1570 (2020).
8. Hecksher, T. et al. Toward broadband mechanical spectroscopy. *Proc. Natl Acad. Sci. USA* **114**, 8710–8715 (2017).
9. Schneider, U., Brand, R., Lunkenheimer, P. & Loidl, A. Excess wing in the dielectric loss of glass formers: a Johari-Goldstein β relaxation? *Phys. Rev. Lett.* **84**, 5560–5563 (2000).
10. Lunkenheimer, P., Wehn, R., Riegger, T. & Loidl, A. Excess wing in the dielectric loss of glass formers: further evidence for a β-relaxation. *J. Non Cryst. Solids* **307-310**, 336–344 (2002).
11. Dixon, P. K., Wu, L., Nagel, S. R., Williams, B. D. & Carini, J. P. Scaling in the relaxation of supercooled liquids. *Phys. Rev. Lett.* **65**, 1108–1111 (1990).
12. Leheny, R. L. & Nagel, S. R. Dielectric susceptibility studies of the high-frequency shape of the primary relaxation in supercooled liquids. *J. Non Cryst. Solids* **235-237**, 278–285 (1998).
13. Menon, N. et al. Wide-frequency dielectric susceptibility measurements in glycerol. *J. Non Cryst. Solids* **141**, 61–65 (1992).
14. Menon, N. & Nagel, S. R. Evidence for a divergent susceptibility at the glass transition. *Phys. Rev. Lett.* **74**, 1230–1233 (1995).
15. Wu, L. Relaxation mechanisms in a benzyl chloride–toluene glass. *Phys. Rev. B* **43**, 9906–9915 (1991).
16. Ngai, K. L. & Paluch, M. Classification of secondary relaxation in glass-formers based on dynamic properties. *J. Chem. Phys.* **120**, 857–873 (2004).
17. Blochowicz, T., Tschirwitz, C., Benkhof, S. & Rössler, E. A. Susceptibility functions for slow relaxation processes in supercooled liquids and the search for universal relaxation patterns. *J. Chem. Phys.* **118**, 7544–7555 (2003).
18. Bauer, T., Lunkenheimer, P., Kastner, S. & Loidl, A. Nonlinear dielectric response at the excess wing of glass-forming liquids. *Phys. Rev. Lett.* **110**, 107603 (2013).
19. Duvvuri, K. & Richert, R. Dielectric hole burning in the high frequency wing of supercooled glycerol. *J. Chem. Phys.* **118**, 1356–1363 (2003).
20. Lunkenheimer, P., Wehn, R., Schneider, U. & Loidl, A. Glassy aging dynamics. *Phys. Rev. Lett.* **95**, 055702 (2005).
21. Diezemann, G., Mohanty, U. & Oppenheim, I. Slow secondary relaxation in a free-energy landscape model for relaxation in glass-forming liquids. *Phys. Rev. E* **59**, 2067–2083 (1999).
22. Domschke, M., Marsilius, M., Blochowicz, T. & Voigtmann, T. Glassy relaxation and excess wing in mode-coupling theory: the dynamic susceptibility of propylene carbonate above and below T_c. *Phys. Rev. E* **84**, 031506 (2011).
23. Sethna, J. P., Shore, J. D. & Huang, M. Scaling theory for the glass transition. *Phys. Rev. B* **44**, 4943–4959 (1991).
24. Stevenson, J. D. & Wolynes, P. G. A universal origin for secondary relaxations in supercooled liquids and structural glasses. *Nat. Phys.* **6**, 62–68 (2010).
25. Viot, P., Tarjus, G. & Kivelson, D. A heterogeneous picture of α relaxation for fragile supercooled liquids. *J. Chem. Phys.* **112**, 10368–10378 (2000).
26. Chamberlin, R. V. Mesoscopic mean-field theory for supercooled liquids and the glass transition. *Phys. Rev. Lett.* **82**, 2520–2523 (1999).
27. Dyre, J. C. & Schrøder, T. B. Universality of a.c. conduction in disordered solids. *Rev. Mod. Phys.* **72**, 873–892 (2000).
28. Berthier, L. & Garrahan, J. P. Numerical study of a fragile three-dimensional kinetically constrained model. *J. Phys. Chem. B* **109**, 3578–3585 (2005).
29. Ninarello, A., Berthier, L. & Coslovich, D. Models and algorithms for the next generation of glass transition studies. *Phys. Rev. X* **7**, 021039 (2017).
30. Berthier, L., Charbonneau, P., Ninarello, A., Ozawa, M. & Yaida, S. Zero-temperature glass transition in two dimensions. *Nat. Commun.* **10**, 1508 (2019).
31. Berthier, L. et al. Configurational entropy measurements in extremely supercooled liquids that break the glass ceiling. *Proc. Natl Acad. Sci. USA* **114**, 11356–11361 (2017).
32. Berthier, L., Flenner, E., Fullerton, C. J., Scalliet, C. & Singh, M. Efficient swap algorithms for molecular dynamics simulations of equilibrium supercooled liquids. *J. Stat. Mech.* **2019**, 064004 (2019).
33. Yu, H.-B., Richert, R. & Samwer, K. Structural rearrangements governing Johari-Goldstein relaxations in metallic glasses. *Sci. Adv* **3**, e1701577 (2017).
34. Illing, B. et al. Mermin–Wagner fluctuations in 2D amorphous solids. *Proc. Natl Acad. Sci. USA* **114**, 1856–1861 (2017).
35. Flenner, E. & Szamel, G. Fundamental differences between glassy dynamics in two and three dimensions. *Nat. Commun.* **6**, 7392 (2015).
36. Berthier, L. & Ediger, M. D. How to 'measure' a structural relaxation time that is too long to be measured? *J. Chem. Phys.* **153**, 044501 (2020).
37. Chandler, D. & Garrahan, J. P. Dynamics on the way to forming glass: bubbles in space-time. *Annu. Rev. Phys. Chem.* **61**, 191–217 (2010).
38. Keys, A. S., Hedges, L. O., Garrahan, J. P., Glotzer, S. C. & Chandler, D. Excitations are localized and relaxation is hierarchical in glass-forming liquids. *Phys. Rev. X* **1**, 021013 (2011).
39. Vogel, M. & Glotzer, S. C. Spatially heterogeneous dynamics and dynamic facilitation in a model of viscous silica. *Phys. Rev. Lett.* **92**, 255901 (2004).
40. Dyre, J. C. Master-equation appoach to the glass transition. *Phys. Rev. Lett.* **58**, 792–795 (1987).
41. Bouchaud, J.-P. Weak ergodicity breaking and aging in disordered systems. *J. Phys. I* **2**, 1705–1713 (1992).
42. Rehwald, C., Rubner, O. & Heuer, A. From coupled elementary units to the complexity of the glass transition. *Phys. Rev. Lett.* **105**, 117801 (2010).
43. Rehwald, C. & Heuer, A. How coupled elementary units determine the dynamics of macroscopic glass-forming systems. *Phys. Rev. E* **86**, 051504 (2012).
44. Arkhipov, V. I. & Baessler, H. Random-walk approach to dynamic and thermodynamic properties of supercooled melts. 1. Viscosity and average relaxation times in strong and fragile liquids. *J. Phys. Chem.* **98**, 662–669 (1994).
45. Scalliet, C., Guiselin, B. & Berthier, L. Excess wings and asymmetric relaxation spectra in a facilitated trap model. *J. Chem. Phys.* **155**, 064505 (2021).
46. Xia, X. & Wolynes, P. G. Microscopic theory of heterogeneity and nonexponential relaxations in supercooled liquids. *Phys. Rev. Lett.* **86**, 5526–5529 (2001).

Methods

Glass-forming computer models. We study a non-additive, continuously polydisperse mixture of spherical particles of equal mass m in two and three dimensions ($d=2$ and $d=3$, respectively)[29]. Two particles i and j, at a distance r_{ij} from one another, interact via the repulsive potential

$$v(r_{ij}) = \epsilon\left(\frac{\sigma_{ij}}{r_{ij}}\right)^{12} + v_c(r_{ij}/\sigma_{ij}) = \epsilon\left(\frac{\sigma_{ij}}{r_{ij}}\right)^{12} + c_0 + c_2\left(\frac{r_{ij}}{\sigma_{ij}}\right)^2 + c_4\left(\frac{r_{ij}}{\sigma_{ij}}\right)^4, \quad (2)$$

if $r_{ij}/\sigma_{ij} < x_c = 1.25$. The constants $c_0 = -28\epsilon/x_c^{12}$, $c_2 = 48\epsilon/x_c^{14}$ and $c_4 = -21\epsilon/x_c^{16}$ ensure continuity of the potential and its first two derivatives at cutoff x_c. The particles' diameters σ_i are distributed from $\mathcal{P}(\sigma) = \mathcal{A}/\sigma^3$, where $\mathcal{A}$ is a normalization constant and $\sigma_{max}/\sigma_{min} = 2.219$. We use the average diameter $\overline{\sigma}$ as the unit length, ϵ as the unit energy (Boltzmann constant is set to unity) and $\sqrt{m\overline{\sigma}^2/\epsilon}$ as the unit time. In these units, $\sigma_{min} = 0.73$ and $\sigma_{max} = 1.62$. We employ a non-additive cross-diameter rule $\sigma_{ij} = 0.5(\sigma_i + \sigma_j)(1 - 0.2|\sigma_i - \sigma_j|)$ to avoid fractionation and crystallization at low temperatures[29]. We simulate the glass-forming model at a number density of particles $\rho = N/L^d = 1$ in a cubic/square box of linear size L using periodic boundary conditions. We consider various system sizes: $N = 1{,}200$ and 10,000 in three dimensions and $N = 2{,}000$ and 10,000 in two dimensions.

Preparation of equilibrated configurations. The model glass-forming liquid is efficiently simulated at equilibrium with the swap Monte Carlo algorithm. We employ the hybrid swap Monte Carlo/MD algorithm implemented in the LAMMPS package (2D/3D) or a home-made code (3D), with optimal parameters, as described in ref. [32]. We prepare $n_s \in [200, 450]$ independent equilibrated configurations at temperatures down to the experimental glass transition temperature.

MD simulations. The equilibrium configurations generated by the swap algorithm are used as the initial conditions for standard MD simulations with integration time step equal to 0.01. In three dimensions, we run conventional constant energy MD (*NVE*) simulations and constant temperature (*NVT*) simulations in two dimensions using a Nosé–Hoover thermostat. The simulations are either run using a home-made MD code or with the LAMMPS package, which allows us to run multi-CPU simulations and perform extremely long runs for relatively large systems (for example, two months on 24 CPUs; Fig. 2).

Relating experimental and numerical timescales. We measure the relaxation time at the onset of glassy dynamics as the reference time, and use this value to translate the numerical timescales into experimental ones. In experiments, many supercooled liquids have $\tau_o \approx 10^{-10}$ s. We measure $\tau_o \approx 3$ in 2D and 3D simulations. In three dimensions, the longest simulation time is $t_{max} = 1.5\times10^7 = 5.0\times10^6\tau_o$. We, therefore, simulate the equilibrium relaxation at T_g over 0.5 ms. In two dimensions, we ran months-long simulations to reach $t^{2D}_{max} = 6\times10^8 = 2\times10^8\tau_o$. Our numerical approach, therefore, allows us to observe the equilibrium dynamics over 20 ms at T_g, which is a giant leap forward in the equilibrium simulations of supercooled liquids.

Average dynamic observables. In three dimensions, we monitor the relaxation dynamics via the self-intermediate scattering function

$$F_s(t) = \left\langle \frac{1}{N}\sum_{i=1}^{N} \cos[\mathbf{q}\cdot\delta\mathbf{r}_i(t)] \right\rangle_{\mathbf{q},n_s}, \quad (3)$$

where $\delta\mathbf{r}_i(t)$ is the displacement of particle i over time t. The brackets indicate the ensemble average over n_s independent runs along with an angular average over wavevectors with $|\mathbf{q}| = 6.9$ (first peak in the total structure factor).

In two dimensions, collective long-ranged fluctuations give rise to a spurious contribution to the displacements of particles[34], which affects the measurement of $F_s(t)$ and makes it ill suited to capture the glassy slowdown. We study the dynamics through the evolution of the local environment of particles, instead of their displacements. We define a bond-orientational correlation function $C_\Psi(t)$ (ref. [35]). We introduce the sixfold bond-orientational order parameter of particle i as

$$\Psi_i(t) = \frac{1}{n_i}\sum_{j=1}^{n_i} e^{i6\theta_{ij}(t)}, \quad (4)$$

where n_i is the number of neighbours of i at time t. Neighbours are particles j with $r_{ij} < 1.45$ (first minimum in the radial distribution function). Alternative definitions of neighbours, for example, via Voronoi tessellation or solid-angle-based method[47], lead to the same quantitative results. Here $\theta_{ij}(t)$ is the angle between the x axis and the axis connecting i and j at time t, without loss of generality owing to rotational invariance. The bond-orientational correlation function is defined as

$$C_\Psi(t) = \left\langle \frac{\sum_i \Psi_i(t)[\Psi_i(0)]^*}{\sum_i |\Psi_i(0)|^2} \right\rangle_{n_s}, \quad (5)$$

where the brackets denote the ensemble average over n_s independent runs and the asterisk is the conjugate complex. In two dimensions, we define the relaxation time as $C_\Psi(\tau_\alpha) = e^{-1}$.

Mobility at the single-particle level. When analysing the mobility at the single-particle level, we first need a criterion to distinguish between mobile and immobile particles. In three dimensions, we have considered several mobility definitions that give quantitatively similar results. The first mobility definition is based on displacements. To remove fast dynamical processes, we use the conjugate gradient method and find the inherent structure (IS) of a configuration at time t, namely, $\{\mathbf{r}_i^{IS}(t)\}$. Particle i is defined as mobile at time t if $|\mathbf{r}_i^{IS}(t) - \mathbf{r}_i^{IS}(0)| > 0.8$ (ref. [48]). This cutoff is between the first minimum and second maximum of the self-part of the Van Hove function $G_s(r,t) = \langle\delta(r - |\mathbf{r}_i^{IS}(t)|)\rangle_{i,n_s}$ in the time regime where $F_s(t)$ is almost constant. This first mobility definition is, however, not convenient in two dimensions because of the collective long-ranged fluctuations that affect the translational dynamics.

A second mobility definition is based on changes in the particle's local environment. At time $t = 0$, we find number n_i and the identity of particle i's neighbours, defined as particles j with $r_{ij}/\sigma_{ij} < 1.485$ in three dimensions (1.300 in two dimensions), corresponding to the first minimum in the rescaled pair correlation function $g(r_{ij}/\sigma_{ij})$. We define the bond-breaking correlation as the fraction of the remaining neighbours at time t:

$$C_B^i(t) = \frac{n_i(t|0)}{n_i}, \quad (6)$$

where $n_i(t|0)$ is the number of particle neighbours of i at $t = 0$ and still neighbours at t. To avoid short-time oscillations in C_B^i caused by particles frequently exiting/entering the neighbour-defining shell, we use a slightly larger cutoff to define the neighbours at $t > 0$, namely, $r_{ij}/\sigma_{ij} < 1.7$ (for $d = 2, 3$). We compute the bond-breaking correlation function as

$$C_B(t) = \left\langle \frac{1}{N}\sum_{i=1}^{N} C_B^i(t) \right\rangle_{n_s}, \quad (7)$$

which is averaged over n_s independent runs.

A particle is defined as mobile at t if $C_B^i(t) < 0.55$, that is, if it has lost half of its initial neighbours. The cutoff value ensures that the set of particles identified as mobile in this way substantially overlap with that identified via the displacement criterion. We then introduce clusters of mobile particles. Two particles i and j that are mobile at time t belong to the same cluster if $r_{ij} < 1.5$ in three dimensions and $r_{ij} < 1.4$ in two dimensions, close to the first minimum of $g(r)$.

Relevant temperature scales. We determine three temperature scales relevant to the glassy slowdown: the onset temperature of glassy dynamics T_o, the mode-coupling crossover temperature T_{mct} below which conventional MD simulations cannot reach equilibrium and the extrapolated experimental glass transition temperature T_g. In three dimensions, $T_o = 0.200$, $T_{mct} = 0.095$ and $T_g = 0.056$. In two dimensions, $T_{o,2D} = 0.20$, $T_{mct,2D} = 0.12$ and $T_{g,2D} = 0.07$. We fit the high-temperature τ_α data to an Arrhenius law, and identify the onset temperature T_o as the temperature below which τ_α is super-Arrhenius. We note $\tau_o = \tau_\alpha(T_o)$. The mode-coupling crossover temperature T_{mct} is obtained by fitting the data with a power law $\tau_\alpha(T) \propto (T - T_{mct})^{-\gamma}$ in the regime $0 \le \log_{10}(\tau_\alpha/\tau_o) \le 3$ (ref. [49]), where $\gamma = 2.7$ and 2.5 for $d = 2$ and 3, respectively. Given that $\log_{10}(\tau_\alpha/\tau_o) \approx 4$ at T_{mct}, this temperature delimits the regime $T > T_{mct}$ (where MD alone can reach equilibrium) from the regime $T < T_{mct}$ (where the swap algorithm is needed to perform equilibrium simulations). The experimental glass transition temperature T_g is defined by $\log_{10}[\tau_\alpha(T_g)/\tau_o] = 12$. In three dimensions, the longest simulation time is $t_{max} = 1.5\times10^7 = 5.0\times10^6\tau_o$; therefore, we can directly access $\log_{10}(\tau_\alpha/\tau_o) \le 7$. We, thus, need to extrapolate our data over five decades to locate T_g. We increase the accuracy of extrapolation by using TTS, which is well obeyed in our model[36]. In the temperature regime where correlation functions reach e^{-1}, the second step of relaxation is well fitted by a stretched exponential $F_0 e^{-(t/\tau_\alpha)^\beta}$. The stretching exponent $\beta \simeq 0.56$ in three dimensions (in two dimensions, $\beta \simeq 0.60$ for C_Ψ and $\beta \simeq 0.67$ for C_B) is almost independent of temperature, and amplitude F_0 slightly increases with decreasing temperature. Fixing β, we estimate τ_α at temperatures where decorrelation is sufficient to perform accurate TTS, extending our measurements over approximately two decades. We extrapolate τ_α over the four remaining decades using an Arrhenius fit $\tau_\alpha(T) \propto e^{E_A/T}$, where $E_A = 2.67$ in three dimensions (2.97 in two dimensions), and locate T_g. Importantly, the Arrhenius extrapolation is a safe choice as it, at worst, underestimates the relaxation times.

Computation of relaxation spectra. The computation of relaxation spectra $\chi''(\omega)$ first requires to differentiate the correlation function with respect to the logarithm of time. We use a first-order finite-difference approximation. Namely, if the configurations are stored at logarithmically spaced times $\{t_k\}_{k=1\ldots n}$, for $k > 1$, we have

$$\frac{dF_s(t_k)}{d\log t} = \frac{F_s(t_k) - F_s(t_{k-1})}{\log(t_k) - \log(t_{k-1})}. \quad (8)$$

The integral in equation (1) is then evaluated as

$$\chi''(\omega) = -\sum_{k=2}^{n} \frac{\mathrm{d}F_s(t_k)}{\mathrm{d}\log t} \frac{\omega t_k}{1+(\omega t_k)^2} \log\left(\frac{t_k}{t_{k-1}}\right). \quad (9)$$

We use the bond-breaking correlation function C_B instead of F_s in two dimensions. In the Supplementary Information, we discuss errors that arise from computing the spectrum when F_s does not decay to zero. We also discuss issues related to statistical noise and a comparison with direct Fourier transforms.

Trap model. We consider traps with energy levels $E>0$ drawn from the exponential power distribution

$$\rho(E) = \frac{\alpha}{E_0 \Gamma(1/\alpha)} \mathrm{e}^{-(E/E_0)^\alpha}, \quad (10)$$

where Γ is the gamma function, and take $E_0=1$ in the following. We assume that the dynamics at temperature T is thermally activated. The energy E of a trap is renewed after a Poisson-distributed timescale of mean $\langle \tau(E) \rangle = \mathrm{e}^{E/T}$. The equilibrium energy distribution at temperature T is

$$P_{\mathrm{eq}}(T,E) = \frac{\rho(E)\mathrm{e}^{E/T}}{Z(T)}, \text{where } Z(T) = \int_0^\infty \mathrm{d}E \rho(E) \mathrm{e}^{E/T}. \quad (11)$$

We monitor the relaxation dynamics by computing the average persistence function $p(t)$. In the absence of dynamic facilitation, the persistence can be directly computed as

$$p(t) = \int_0^\infty \mathrm{d}E P_{\mathrm{eq}}(T,E) \mathrm{e}^{-t/\langle \tau(E) \rangle}. \quad (12)$$

In the absence of dynamic facilitation, the average persistence is evaluated using Mathematica (NIntegrate and WorkingPrecision of 30). We then calculate the relaxation spectrum $\chi''(\omega)$ by following the procedure described previously, replacing $F_s(t)$ with persistence $p(t)$. We compute persistence $p(t)$ over a time interval large enough to observe full decorrelation, namely, $[10^{-10}, 10^{70}]$, for $\alpha=1.1$ and $T=0.629$, and minimize errors in the relaxation spectrum.

Simulations of the facilitated trap model. We consider a system composed of N traps. We initialize the simulation with an equilibrium condition by sampling the traps' energies directly from the equilibrium distribution $P_{\mathrm{eq}}(T,E)$. Since the cumulative probability distribution of energies $\mathcal{C}_{\mathrm{eq}}$ cannot be explicitly computed, we use Mathematica to evaluate it, and to numerically construct the reciprocal function $\mathcal{E} = \mathcal{C}_{\mathrm{eq}}{}^{-1}$. For each of the N traps, we generate X uniformly distributed in $[0,1]$, and assign it an energy $E = \mathcal{E}(X)$. This procedure generates an initial condition in equilibrium. Each trap is assigned a renewal time exponentially distributed, with mean $\mathrm{e}^{E/T}$. We initialize persistence $p_i(t=0)$ of all the traps to one.

The dynamics proceeds as follows. First, we identify trap i_o with the smallest renewal time τ_{min}, which will relax first. We update all the other traps by subtracting τ_{min} to their renewal time τ_i. When the trap i_o relaxes, its persistence is set to zero, that is, $p_{i_o}=0$, and we give it a new energy value sampled from $\rho(E)$, as well as a new renewal time, as described above.

This relaxation event then affects all the other traps. We attempt to displace their energy by a random amount δE (different for each trap) uniformly distributed in $\left[-\frac{4}{\sqrt{N}}, \frac{4}{\sqrt{N}}\right]$: $E \to E' = E + \delta E$. The scaling with N ensures that the resulting dynamics is independent of N. We then accept or reject this attempt to leave the equilibrium probability distribution P_{eq} unchanged. To this end, we introduce an effective potential $V = -T \log P_{\mathrm{eq}}$, and compute the change in effective potential $\delta V = T(E'^{\alpha} - E^{\alpha}) - \delta E$. We then use the Metropolis filter: if $\delta V < 0$, the change in energy is accepted; otherwise, it is accepted with probability $\exp(-\delta V/T)$. When accepted, we pick a new renewal time exponentially distributed with average $\mathrm{e}^{E'/T}$. When the move is completed, we again determine which of the traps is the next one to relax, and proceed as before.

We measure the average persistence $p(t) = \left\langle \sum_i p_i(t)/N \right\rangle$, where the brackets indicate average over independent runs, and where the sum runs over all the traps. We simulate the dynamics of the model until the total persistence is equal to zero.

Data availability

Source data are provided with this paper. The data that support the findings of this study are available from the corresponding author upon reasonable request.

Code availability

The codes used in this study are available from the corresponding author upon reasonable request.

References

47. van Meel, J. A., Filion, L., Valeriani, C. & Frenkel, D. A parameter-free, solid-angle based, nearest-neighbor algorithm. *J. Chem. Phys.* **136**, 234107 (2012).
48. Schrøder, T. B., Sastry, S., Dyre, J. C. & Glotzer, S. C. Crossover to potential energy landscape dominated dynamics in a model glass-forming liquid. *J. Chem. Phys.* **112**, 9834–9840 (2000).
49. Götze, W. *Complex Dynamics of Glass-Forming Liquids: A Mode-Coupling Theory* Vol. 143 (Oxford Univ. Press, 2009).

Acknowledgements

We thank G. Biroli, M. Ediger and J. Kurchan for discussions, and S. Nagel for detailed explanations about the experiments. Some simulations were performed at MESO@LR platform at the University of Montpellier. This work was supported by a grant from the Simons Foundation (no. 454933; L.B.), the European Research Council under the EU's Horizon 2020 programme via grant no. 740269 (C.S.), a Herchel Smith Postdoctoral Research Fellowship (C.S.), a Ramon Jenkins Research Fellowship from Sidney Sussex College, Cambridge (C.S.), and Capital Fund Management - Fondation pour la Recherche (B.G.).

Author contributions

B.G., C.S. and L.B. designed the research. B.G. and C.S. carried out the simulations. B.G, C.S. and L.B. analysed the data and wrote the paper.

Competing interests

The authors declare no competing interests.

Additional information

Supplementary information The online version contains supplementary material available at https://doi.org/10.1038/s41567-022-01508-z.

Correspondence and requests for materials should be addressed to Ludovic Berthier.

Peer review information *Nature Physics* thanks Reiner Zorn, Thomas Voigtmann and the other, anonymous, reviewer(s) for their contribution to the peer review of this work.

Reprints and permissions information is available at www.nature.com/reprints.